Catalysis Letters Vol. 101, Nos. 1–2, May 2005 (© 2005)
DOI: 10.1007/s10562-004-3753-x

In situ Ga K edge XANES study of the activation of Ga/ZSM-5 prepared by chemical vapor deposition of trimethylgallium

Emiel J.M. Hensen[a,*], Mayela García-Sánchez[a], Neelesh Rane[a], Pieter C.M.M. Magusin[a], Pang-Hung Liu[b], Kuei-Jung Chao[b], and R.A. van Santen[a]

[a]*Schuit Institute of Catalysis, Eindhoven University of Technology, P.O. Box 513, 5600, MB, Eindhoven, The Netherlands*
[b]*Department of Chemistry, National Tsinghua University, Kuang Fu Road, Hsinchu 30043, Taiwan, ROC*

Received 6 November 2004; accepted 3 December 2004

The activation of a dimethylgallium/ZSM-5 precursor to well-defined reduced and oxidized species is studied by *in situ* Ga K edge XANES. The precursor is prepared by chemical implanting of trimethylgallium on acidic HZSM-5. Subsequent reduction leads to charge-compensating Ga^+ species. Direct oxidation of the trimethylgallium precursor leads to various forms of gallium oxide and regeneration of Brønsted acid protons. Oxidation of the reduced Ga^+ species yields predominantly to GaO^+ species. The GaO^+ species exhibit a much higher H_2/D_2 exchange activity than reduced Ga^+ species.

KEY WORDS: dehydrogenation; EXAFS; FTIR; gallium; HZSM-5; XANES; zeolite.

1. Introduction

Gallium dispersed in acid materials can be applied to dehydrogenate alkanes. In combination with the shape-selective properties of a medium-pore zeolite such as ZSM-5, light paraffins can be converted into aromatic hydrocarbons including benzene, toluene and xylenes. A commercial application is found in the Cyclar process [1,2]. The reaction mechanism is thought to consist of a complex scheme involving dehydrogenation, oligomerization and ring-closure steps. Despite considerable research efforts in the area of Ga-containing zeolites [3–11], the exact role of gallium in this mechanism has not been totally elucidated yet, with proposals for its role as dehydrogenation function in a pure bifunctional [3–6] or concerted mechanism [7] and as a promoter to recombinative hydrogen removal during alkane dehydrogenation on Brønsted acid sites [8–11] receiving most attention. The structure of the active intrazeolite Ga species and their reactivity in oxidative and reductive conditions has not been fully resolved yet, owing to the wide variety of possible structures including bulk Ga_2O_3 aggregates on the external zeolite surface, small gallium oxide aggregates occluded in the zeolite micropore space, reduced Ga species such as Ga_2O and cationic Ga species in oxidized or reduced form. Various methods to incorporate extra-framework gallium into the micropore space of HZSM-5 have been described [12] including impregnation [13,14] and ion-exchange [15] with Ga^{3+} salts, physical mixing with Ga_2O_3 [16] and chemical vapor deposition (CVD) of $GaCl_3$ [17,18]. Impregnation, ion-exchange and physical mixing lead to poorly dispersed gallium oxide species, mostly present on the external zeolite surface. The dispersion can be increased by reduction of the gallium oxide [12], resulting in the formation of Ga^+ species [14,16] or GaH_2^+ species [14] compensating the zeolite framework charge. The role of these reduced Ga^+ species with respect to dehydrogenation is not clear [16,19]. However, the reduction to Ga^+ entities goes with a decrease in the Brønsted acidity [5,14], which will in turn strongly affect the overall performance in hydrocarbon reactions. The hydrolysis step after CVD of gallium chloride also leads to a variety of Ga species including GaO^+ cations and Ga_2O_3 species [18,20].

In order to prepare better-defined Ga species in medium-pore zeolites we have recently examined the CVD of trimethylgallium (TMG) in HZSM-5 and HMOR [21]. In short, TMG can effectively replace the Brønsted acid protons in HZSM-5, resulting in mononuclear dimethylgallium species. Here, we report an *in situ* X-ray absorption near-edge spectroscopy (XANES) study of the thermal activation of these species. Activation was carried out by reduction with molecular hydrogen because this results in better-defined species compared to an oxidative pretreatment [21]. Nevertheless, we will also address the oxidation of the zeolite-occluded gallium alkyl species. A previous Ga K edge XAS study [10] indicated that the oxidation state of the reduced Ga species changes upon cooling indicating that *in situ* studies at relatively high temperatures are a prerequisite. Therefore, we studied the catalytic materials by XANES under conditions relevant to catalysis.

* To whom correspondence should be addressed.
E-mail: E.J.M.Hensen@tue.nl

2. Experimental

2.1. Preparation

TMG/ZSM-5 catalyst was synthesized by CVD of TMG (Aldrich, 99%) on HZSM-5 zeolite. To a glass vessel containing well-dried HZSM-5 zeolite (Akzo Nobel, Si/Al = 19.4), 1 ml of TMG was added in an Ar-flushed glove-box. After 24 h, the resulting material was evacuated for 2 h to remove unreacted TMG and gaseous reaction products, mainly methane. The resulting material was kept in argon atmosphere prior to XANES characterization. The gallium loading was found to be 6.8 wt% by ICP analysis.

2.2. Characterization

X-ray absorption spectra were recorded at beamline BL17C of the National Synchrotron Radiation Research Center (NSRRC), Taiwan. The storage ring energy was operated at 1.5 GeV with the beam current between 120 and 200 mA. Absorption spectra were measured in transmission mode. The energy was scanned from 200 and 20 eV below the Ga K absorption edge (10,367 eV) to 1000 and 60 eV above the edge for EXAFS analysis and *in situ* XANES experiments, respectively. Standard Ga_2O_3 powder was used as a reference and measured simultaneously with the sample. Samples were mounted in an controlled atmosphere transmission cell under exclusion of contact with air. The as-prepared sample was reduced in a flow of 100 ml min^{-1} (20 vol% hydrogen in helium) at a rate of 4 K min^{-1} to 773 K. After an isothermal period of 10 min, the cell was flushed with He. Subsequently, the sample was exposed to a flow of 100 ml min^{-1} of 20 vol% oxygen in helium for 10 min, followed again by a reduction at this temperature for 10 min. During these steps, near-edge spectra were recorded at regular time intervals. For some catalysts, EXAFS spectra were recorded after cooling to room temperature. The data analysis was carried out with the UWXAFS 3.0 and FEFF8 software packages. Structural information was determined by multiple-shell fitting in *R*-space. Both k^2- and k^3-weighted Fourier transformation without phase correction were performed. As input to FEFF8, a known atom cluster from the reference β-Ga_2O_3 compound and interatomic distances from the published crystal structure were used [22].

FTIR spectroscopy was carried out with a Bruker IFS113v spectrometer in a controlled atmosphere transmission cell. A wafer of approximately 10 mg of TMG/ZSM-5 was pressed and loaded into the cell. Spectra were recorded for TMG/ZSM-5 after evacuation for 120 min, after reduction at 823 K or after oxidation at 823 K. The spectrum of the dehydrated parent HZSM-5 material is given for comparison.

^{27}Al MAS NMR measurements were carried out on a Bruker DMX500 spectrometer operating at 130.3 MHz. The sample was rotated in a 4 mm rotor with a spin rate of 12.5 kHz. Single-pulse excitation was used with a 30° pulse of 1.5 μs. Thousand scans were accumulated with a time resolution of 5 μs (100 kHz spectral width) and interscan delay of 1 s. A solution of $Al(NO_3)_3$ was used for shift calibration.

2.3. H_2/D_2 equilibration

Hydrogen–deuterium exchange was measured in a quartz batch reactor equipped with a quadrupole mass spectrometer (Balzers QMS 200 M system). Prior to reaction, the catalyst was loaded and pretreated in hydrogen or oxygen whilst heating from room temperature to 773 K at a heating rate of 2 K min^{-1}. During pretreatment, the evolution of decomposition gases of the precursor was followed by the mass spectrometer. After evacuation and cooling to the reaction temperature of 573 K, equimolar amounts of hydrogen, deuterium and nitrogen (each 1 kPa) were admitted to reactor. The evolution of the reaction gases (H_2, D_2 and HD) was followed by the mass spectrometer for 20 h.

3. Results and discussion

Fourier transforms of k^3-weighted EXAFS spectra of the Ga_2O_3 reference, the as-synthesized TMG/ZSM-5 and the material after reduction and oxidation are compared in figure 1. Table 1 lists the corresponding EXAFS fit parameters. The structure analysis of the

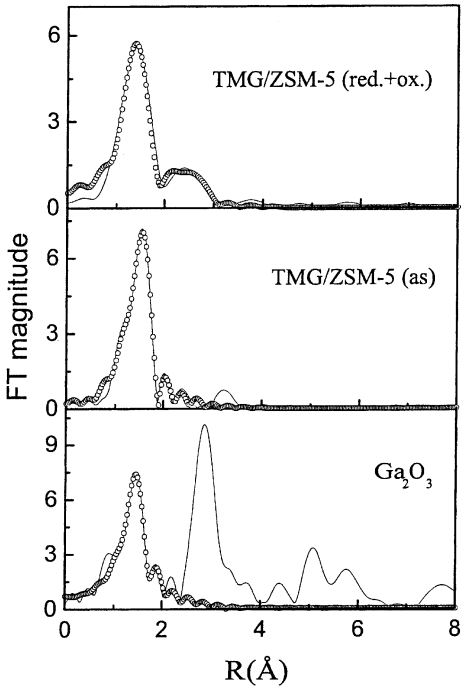

Figure 1. Fourier transforms of Ga K edge k^3-weighted EXAFS data. Solid lines and open circles are the experimental and the fitted results, respectively. Note that the phase shifts were not corrected.

Table 1
Fitting parameters of EXAFS data at the Ga K edge

Sample	Shell	C.N.	R (Å)	σ^2 (Å^2) $\times 10^{-3}$
Ga_2O_3	Ga–O	1.7	1.86	4
	Ga–O	3.1	1.99	13
TMG/ZSM-5(as)	Ga–C	1.9	1.95	15
	Ga–O	1.0	1.82	2
TMG/ZSM-5	Ga–O	0.7	1.81	1
(red. + ox.)-I	Ga–O	2.3	1.98	8
	Ga–Al	0.8	2.90	9
TMG/ZSM-5	Ga–O	4.0	1.83	8
(red. + ox.)-II	Ga–Al	1.3	3.07	6

Ga_2O_3 reference compound indicates a ratio of Ga(t)/Ga(o) = (1.7/4)/(3.1/6) ≈ 0.8. This ratio is calculated from the coordination number of Ga–O bonds with a Ga(t)–O bond distance of R = 1.86 Å (tetrahedral Ga) and a Ga(o)–O distance of R = 1.99 Å (octahedral Ga) in good agreement with earlier EXAFS and XRD studies [23,24]. The data are also in good agreement with a separate XANES analysis of the edge, giving Ga(t)/Ga(o) = 0.73. The lower than unity ratio suggests that the reference is not a ideal β-form of Ga_2O_3 [25,26].

The as-synthesized sample contains Ga atoms coordinating to oxygen and carbon atoms. Although we earlier calculated a minimum-energy configuration of dimethylgallium coordinating to two zeolite framework oxygen atoms [21], the present EXAFS fit parameters point to the coordination of the dimethylgallium species to a single oxygen atom. This suggests that the Ga-alkyl species binds more strongly to one of the oxygen atoms while a weaker bond with the other surrounding oxygen atoms may not be detected by EXAFS. The Ga–C bond distance of R = 1.95 Å is in good agreement to values around 1.96 Å obtained for TMG [27,28]. There is also a backscatterer visible at R = 2.92 Å which is most probably due to Ga–Si and Ga–Al.

Figure 2 displays XANES spectra of TMG/ZSM-5 materials during *in situ* reduction. We infer that the distinct absorption feature in as-synthesized TMG/ZSM-5 belongs to $O_{zeolite}$–$Ga(CH_3)_2$ species. The lower edge energy of the dimethylgallium species coordinating to the zeolite framework compared to the reference compound is caused by the presence of the two alkyl groups which results in a partial reduction of Ga^{3+}. The other weaker absorption maximum around 10,381 eV might be due to Ga-alkyl species interacting with silanol groups. The XANES spectra during reduction of TMG/ZSM-5 do not point to large changes of the gallium oxidation state up to a temperature of about 650 K. At this temperature, the maximum of the absorption feature at 10,375 eV shifts to lower energies and the maximum of the absorption feature around 10,381 eV shifts to 10,379 eV. The shift of the edge energy during the reductive treatment can be followed in figure 3. The edge energy is constant (10,373 eV) up to a temperature

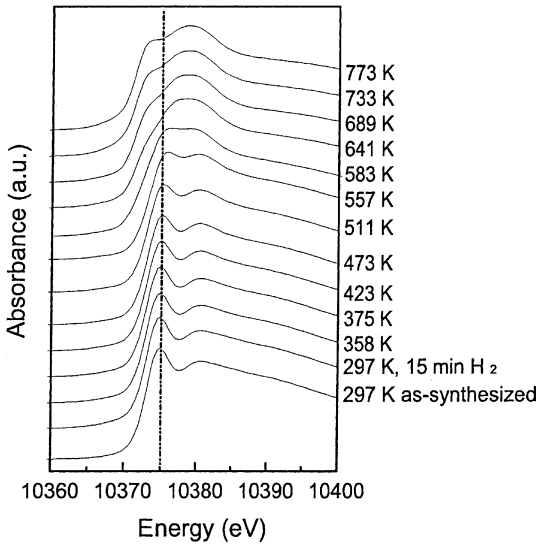

Figure 2. Ga K edge XANES spectra of the as-synthesized TMG/ZSM-5 material and of the materials at various stages during temperature-programmed reduction in 20 vol% H_2 in helium.

of 640 K and then shifts to lower energy (10,371.5 eV). During further reduction at 773 K, the edge energy does not change anymore. We attribute the shift in edge energy to the reduction of dimethylgallium to monovalent Ga^+ species. The other Ga species can only be slightly reduced as is evident from the decrease of the absorption maximum to 10,379 eV similar to earlier work on Ga-beta [22].

The reduction process is further monitored by a separate temperature-programmed reduction experiment. Figure 4 shows the evolution of methane as a function of temperature. We observe a small feature around 400 K which we tentatively attribute to some further reaction of physisorbed TMG with remaining

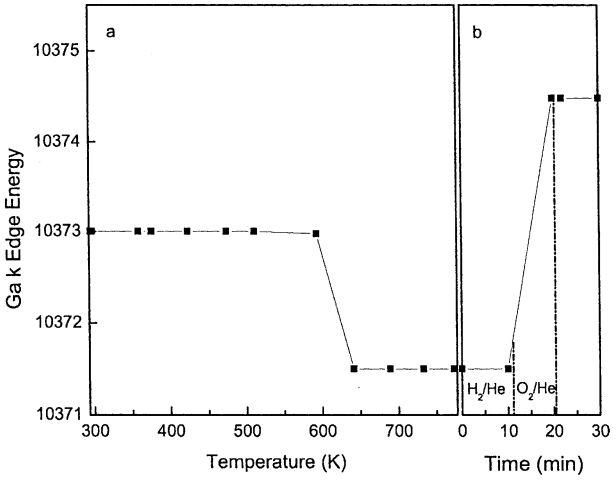

Figure 3. Evolution of Ga K edge energy during (a) temperature-programmed reduction in 20 vol% H_2 in helium and (b) subsequent isothermal (773 K) treatments in hydrogen, oxygen and hydrogen again.

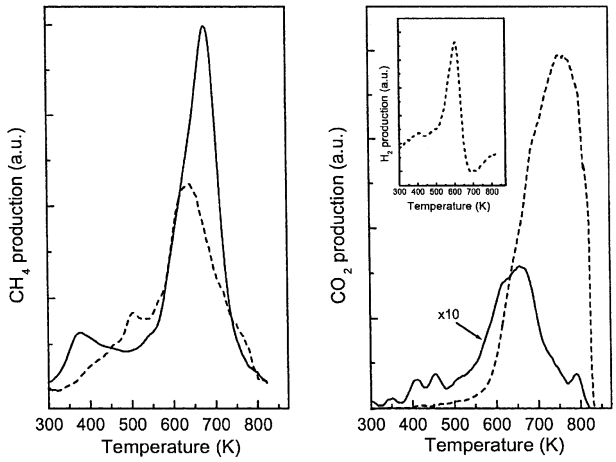

Figure 4. Production of methane (left) and carbon dioxide (right) as a function of temperature in hydrogen (full line) or oxygen (dashed line). The inset shows the hydrogen production during oxidation.

hydroxyl groups. A main production peak of methane with a maximum at 673 K is also observed. Methane production already starts around 600 K. These results are in good agreement with the shift of the edge energy around 640 K. Moreover, we observed the production of very small amounts of ethane, propane and carbon dioxide (alkanes typically two orders of magnitude lower than the amount of methane, carbon dioxide three orders of magnitude lower) during the reductive decomposition of the precursor. We speculate that gallium is present as monovalent Ga^+ species since we have recently found GaH_2^+ species is not stable under the present reaction conditions [14]. Upon oxidation, mainly carbon dioxide and water is produced around 773 K with small amounts of hydrocarbons, mostly ethane, and hydrogen being released at lower temperatures. This suggests that the alkyl groups eliminated as hydrocarbons and can be dehydrogenated giving hydrogen and coke depositions that are burned at higher temperatures. The coke deposition is confirmed by the observation that the material has turned black below 773 K. The subsequent oxidation of this coke deposit results in the formation of carbon dioxide and water. This also provides an explanation for the higher amount of extraframework Al species derived from the higher intensity of the resonance around 0 ppm for oxidized TMG/ZSM-5 compared to the reduced precursor in the ^{27}Al NMR spectra (figure 5). We also observe that the vapor deposition of TMG only leads to a small degree of dealumination but that subsequent activation and most prominently oxidation increases the amount of octahedral Al species. The reduced catalyst also has some distorted (penta-coordinated) Al species between the sharper resonances at 54 and 0 ppm. This could be due to close interaction with reduced Ga species. One has to be careful with the interpretation of these ^{27}Al NMR spectra because they were recorded after re-exposure to air. This will particularly affect the as-synthesized and reduced catalysts. This could also explain the larger difference in dealumination degree as derived from infrared spectroscopy compared to ^{27}Al NMR (*vide infra*).

Meitzner *et al.* [10] reported the formation of reduced Ga species on Ga/HZSM-5 prepared by impregnation of gallium nitrate followed by air calcination upon reduction at 780 K. Clearly, the gallium alkyl precursor can be reduced at a considerably lower temperature than the gallium oxide one. Figure 6 presents XANES spectra of the material after reduction at 773 K and subsequent oxidative and reductive treatments at 773 K. One observes that oxidation at 773 K leads to dramatic changes in the XANES region. The edge energy shifts to a value of 10,374.5 eV indicating the oxidation of the Ga species to Ga^{3+}. We surmise that the oxidation of monovalent Ga^+ results in the formation of $[GaO]^+$, although one should also consider the possibility that small gallium oxide clusters form concomitant with the regeneration of acid protons. Dooley *et al.* [15] have shown that oxidation of reduced Ga species is fast at 823 K but does not proceed to β-Ga_2O_3. The difference in reducibility between the dimethylgallium precursor and the oxidized Ga species is expressed by the minor extent of reduction of the latter species upon exposure to hydrogen at 773 K. Figure 6 shows that such treatment only leads to a weak shoulder on the low energy side indicating that the oxidized species cannot be reduced easily under these conditions. We also performed an EXAFS analysis of the oxidized sample that was additionally reduced for 10 min. The structural parameters of TMG/ZSM-5(red. + ox.) are given in table 1. We could fit these data with two models. In the first coordination shell of model I, we find three oxygen atoms, two oxygen atoms at a distance of $R = 1.98$ Å which we attribute to coordination of Ga to the framework oxygen atoms and one shorter bond with $R = 1.80$ Å. This could be due to a terminal oxygen atom that is

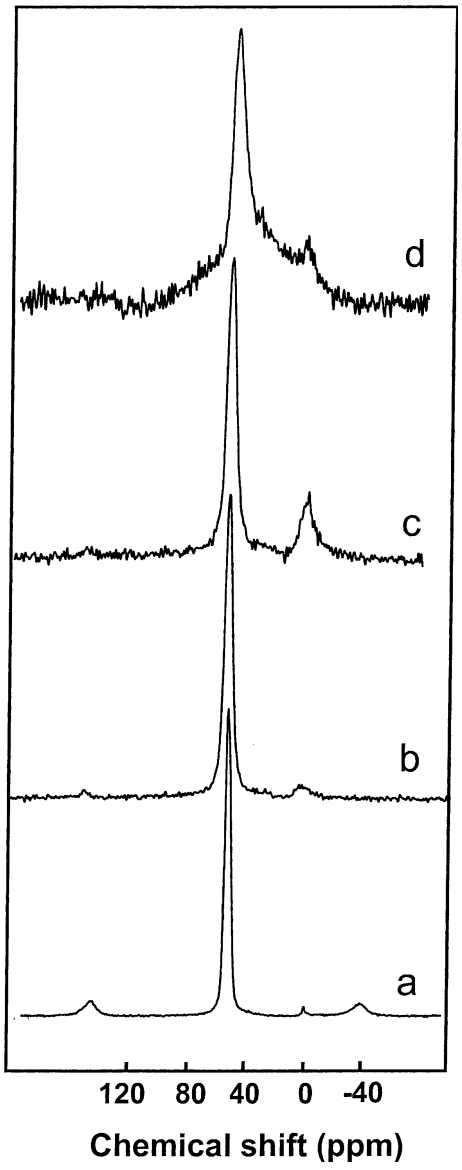

Figure 5. ^{27}Al NMR spectra of (a) parent HZSM-5, (b) as-synthesized TMG/ZSM-5, (c) oxidized TMG/ZSM-5 and (d) reduced TMG/ZSM- 5.

more strongly bonded to the Ga^{3+} atom than the two zeolite oxygen atoms. The structural parameters for the oxidized material cohere well with our surmise that the larger part of gallium is present as $[Ga^{3+} = O^{2-}]^{+}$ (gallyl) species coordinating to the negative framework charge of the zeolite. We also identified a Ga–Al (Ga–Si) backscatterer which is in line with the coordination of the GaO^{+} species to the zeolite framework. On the other hand, we could also produce a satisfactory fit with four oxygen atoms at a distance of $R = 1.83$ Å and a Ga–Al coordination at $R = 3.07$ Å. This latter result could point to the presence of charge-compensating $Ga(OH)_2^{+}$ instead of GaO^{+} species but in principle could also be interpreted in terms of reinsertion of Ga into the zeolite framework.

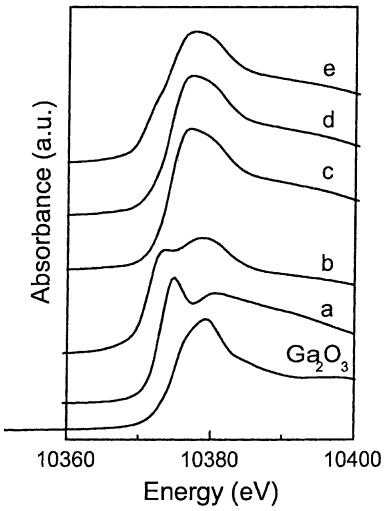

Figure 6. Ga K edge XANES spectra of the Ga_2O_3 reference and (a) as-synthesized TMG/ZSM-5 followed by temperature-programmed reduction and successive treatments at 773 K, (b) reduction in hydrogen for 10 min, (c) further oxidation in 20 vol% O_2 in helium for 10 min and further reduction in hydrogen for (d) 2 min and (e) 10 min.

A comparison of the FTIR spectra of the parent HZSM-5 material and the as-synthesized material (figure 7) shows that TMG has reacted with all hydroxyl groups, i.e. the Brønsted acid hydroxyl groups (3610 cm^{-1}), the hydroxyl groups related to extra-framework Al (3665 cm^{-1}) and the silanol groups (3740 cm^{-1}) in line with an earlier analysis [21]. A direct oxidative treatment results in considerable regeneration of Brønsted acid protons and a substantial regeneration of the silanol groups. The regeneration of about 60% of

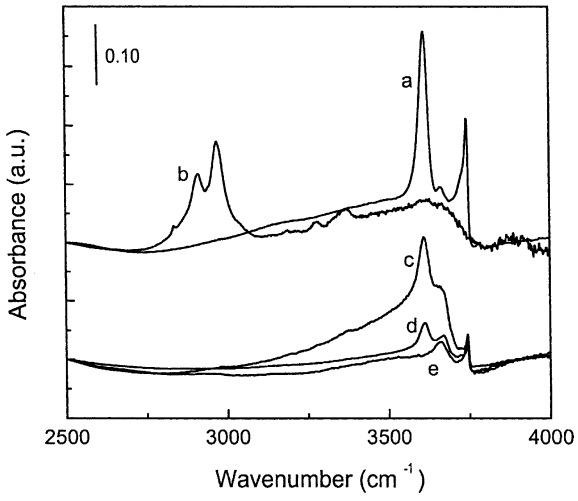

Figure 7. FTIR spectra of parent and modified HZSM-5 catalysts. Spectrum (a) and (b) show the spectra of the dehydrated parent HZSM-5 catalyst and after subsequent CVD of TMG for 1 h and evacuation (TMG/ZSM-5), respectively. The lower three spectra show the hydroxyl region after oxidation of TMG/ZSM-5 after (c) oxidation at 823 K, (d) reduction at 823 K followed by oxidation at 823 K and (e) reduction at 823 K.

the original amount of bridging hydroxyl groups indicates that a considerable amount of the gallium species has been transformed into neutral gallium oxide species occluded in the zeolite micropores as small or on the external surface as larger aggregates. Moreover, we note that the band related to hydroxyl groups coordinating to extraframework Al species has increased considerably and is higher than in the original material. This points to extensive dealumination during the oxidative treatment deriving from steaming effects by water produced at elevated temperatures produced by oxidation of hydrocarbons or hydrocarbon residue. The band also appears to be broader which might relate to the occurrence of hydroxyl groups coordinating to extraframework Ga ions that give rise to a vibrational band around 3680 cm^{-1}. The IR spectrum of the reduced material shows no regeneration of the acid protons suggesting that all exchange sites are occupied by reduced Ga species. The final spectrum is the one of a catalyst that was oxidized at 823 K after reduction of TMG/ZSM-5. The spectrum resembles that of oxidized TMG/ZSM-precursor albeit that the extent of regeneration of Brønsted acid protons amounts to about 15% which is considerably lower than after direct oxidation. This indicates that the latter sample predominantly contains $[GaO]^+$ species. One also observes a band due to OH groups on extraframework Ga species which could mean that part of the charge-compensating ions are present in the form of $Ga(OH)_2^+$ species. Table 2 shows the hydrogen–deuterium equilibration activities of HZSM-5 and reduced and oxidized TMG/ZSM-5 at a reaction temperature of 573 K. Clearly, gallium acts as a promoter for the isotopic exchange between H_2 and D_2 compared to the HZSM-5 parent zeolite. However, oxidized TMG/ZSM-5 shows a three-fold higher activity than the reduced material. This suggests that the reduced Ga^+ species exhibit a lower reactivity in hydrogen activation than gallium oxide species. It is difficult to ascertain whether the higher activity of the oxidized materials should be attributed to $[GaO]^+$ species or gallium oxide microaggregates. To obtain more insight into this, we compared the equilibration activities of two oxidized materials, i.e. the first one obtained during direct oxidation of TMG/ZSM-5 and the second one obtained after oxidation of the reduced precursor.

Table 2
Hydrogen–deuterium equilibration activities (initial HD formation rate) (initial H_2 and D_2 and N_2 partial pressures: 1 kPa; total pressure 3 kPa; T = 573 K)

Catalyst	Pretreatment	Rate (g HD/g cat h)	Rate (mol HD/mol Ga h)
HZSM-5	–	5.0	–
TMG/ZSM-5	reduced	9.9	0.6
	oxidized	30	1.6
	red. + ox.	62	3.3

From the considerably higher activity of the catalyst that contains a lower amount of Brønsted acid protons and hence a higher fraction of cationic species, we infer that $[GaO]^+$ species exhibit a higher activity than the small gallium oxide clusters. This may be simply related to the higher dispersion of the mononuclear Ga species. Recently, we have shown that GaH_2^+ species may form upon exposure of Ga^+ species following

$$ZO^- \cdots Ga^+ + H_2 \leftrightarrows ZO^- \cdots GaH_2^+,$$

where ZO^- stands for the anionic exchange site of the zeolite [14]. Two hydride ions coordinate to tervalent Ga species yielding a positively-charged cationic complex.

These species were shown to occur under the conditions applied for the isotopic exchange reaction [14]. Moreover, they form relatively slowly and are stable up to high temperature. Apparently, the dissociation of hydrogen on the GaO^+ species via

$$ZO^- \cdots GaO^+ + H_2 \leftrightarrows ZO^- \cdots HGaOH^+$$

proceeds faster. This also has implications for the activation of paraffinic hydrocarbons. Heterolytic dissociation of hydrocarbons over GaO^+ species may be preferred over the homolytic dissociation over Ga^+ species. First-principles calculations of Frash and van Santen [29] indicate that ethane activation is most likely to occur on GaH_2^+ species. However, recent experimental findings [14] show that GaH_2^+ species are not stable and decompose to Ga^+ species at typical reaction temperatures (T = 823 K). We surmise that the rate of alkane activation over Ga^+ is small, most likely due to the weak interaction of Ga^+ with hydrocarbons. On the other hand, the activation of a hydrocarbon like ethane over GaO^+ species may occur via a $[GaHOC_2H_5]^+$ intermediate which decomposes into ethylene and $[GaHOH]^+$. The activation energy for the regeneration of the gallyl (GaO^+) ion from the latter species was calculated to be very high [29]. We surmise that desorption of water under reductive conditions is more likely, leading to the formation of Ga^+ species rather than regeneration of GaO^+ species.

4. Conclusions

The adsorption of $Ga(CH_3)_3$ on HZSM-5 results in the formation of chemisorbed $Ga(CH_3)_2^+$ cations. These chemisorbed $Ga(CH_3)_2^+$ ions replace the Brønsted acid protons. An EXAFS structure analysis of the as-synthesized material shows that a dimethylgallium species is formed that coordinates to the zeolite framework. *In situ* XANES data shows that the reduction of these Ga–alkyl species starts around 640 K and leads to the formation of reduced Ga^+ species. The oxidation of these reduced species occurs very fast in the presence of molecular oxygen, mostly leading to Ga^{3+} species in the form of GaO^+ coordinating to the zeolite

framework. These GaO^+ species display a higher activity in hydrogen–deuterium exchange than reduced Ga^+ species.

Acknowledgments

One of us (EH) thanks the Technology Foundation STW, the applied science division of NWO and the technology programme of the Ministry of Economic Affairs for financial support.

References

[1] J.R. Mowry, R.F. Anderson and J.A. Johnson, Oil Gas J. 83 (1985) 1288.
[2] C. Doolan and P.R. Pujado, Hydrocarbon Proc. 68–69 (1989) 72.
[3] Kitagawa, Y. Sendoda and Y. Ono, J. Catal. 101 (1986) 12.
[4] N.S. Gnep, J.Y. Doyemet and M. Guisnet, J. Mol. Catal. 45 (1988) 281.
[5] M. Guisnet, N.S. Gnep and F. Alario, Appl. Catal. A: General 89 (1992) 1.
[6] B.S. Kwak, W.M.H. Sachtler and W.O. Haag, J. Catal. 149 (1994) 465.
[7] B.S. Kwak and Sachtler W.M.H., J. Catal. 145 (1994) 456.
[8] J. Yao, R. Mao and L. Dufresne, Appl. Catal. A: General 65 (1990) 175.
[9] E. Iglesia, J.E. Baumgartner and G.L. Price, J. Catal. 134 (1992) 549.
[10] G.D. Meitzner, E. Iglesia, J.E. Baumgarnter and E.S. Huang, J. Catal. 140 (1993) 209.
[11] J.A. Biscardi and E. Iglesia, Catal. Today 31 (1996) 207.
[12] R. Fricke, H. Kosslick, G. Lischke and M. Richter, Chem. Rev. 100 (2000) 2303.
[13] V.R. Choudhary, K. Mantri and C. Sivadinarayama, Microporous Mesoporous Mater. 37 (2000) 1.
[14] V.B. Kazansky, I.R. Subbotina, R.A. Santen and E.J.M. Hensen, J. Catal. 227 (2004) 263.
[15] K.M. Dooley, C. Chang and G.L. Price, Appl. Catal. A: General 84 (1992) 17.
[16] G.L. Price and V. Kanizirev, J. Catal. 126 (1990) 267.
[17] B.S. Kwak and W.M.H. Sachtler, J. Catal. 141 (1993) 729.
[18] El.-M. El Malki, R.A. Santen and W.M.H. Sachtler, J. Phys. Chem. B 103 (1999) 4611.
[19] R.J. Nash, M.E. Dry and C.T. O'Conner, Appl. Catal. A: General 134 (1996) 285.
[20] B.S. Kwak and W.M.H. Sachtler, J. Catal. 141 (1993) 729.
[21] M. Garcia-Sanchez, P.C.M.M. Magusin, E.J.M. Hensen, P.C. Thüne, X. Rozanska and R.A. Santen, J. Catal. 219 (2003) 352.
[22] A.C. Wei, P.-H. Liu, K.-J. Chao, E. Yang and H.Y. Cheng, Microporous Mesoporous Mater. 47 (2001) 147.
[23] K.-J. Chao, A.C. Wei, H.C. Wu and J.F. Lee, Microporous Mesoporous Mater. 35–36 (2000) 413.
[24] S.J. Geller, Chem. Phys. 33 (1960) 676.
[25] K. Nishi, K.I. Shimizu, M. Tahamatzu, H. Yoshida, A. Satsuma, T. Ranaka, S. Yoshida and T. Hattori, J. Phys. Chem. B 102 (1998) 10190.
[26] K. Shimizu, M. Takamatsu, K. Nishi, H. Yoshida, A. Satsuma, T. Tanaka, S. Yoshida and T. Hattori, J. Phys. Chem. B 103 (1999) 1542.
[27] N.W. Mitzel, C. Lustig, R.J.F. Berger and N. Runeberg, Angew. Chem. Int. Ed. (2002) 41.
[28] R. Boese, A.J. Downs, T.M. Greene, A.W. Hall, C.A. Morrison and S. Parsons, Organometallics 22 (2003) 2450.
[29] M. Frash and R.A. Santen, J. Phys. Chem. A 104 (2000) 2468.